Published in final edited form as:

Struct Multidiscipl Optim. 2010 October ; 42(4): 633–644. doi:10.1007/s00158-010-0508-8.

Topology Optimization of Three Dimensional Tissue Engineering Scaffold Architectures for Prescribed Bulk Modulus and Diffusivity

Heesuk Kang,

Department of Mechanical Engineering, Scaffold Tissue Engineering Group, Department of Biomedical Engineering, Spine Research Laboratory, Department of Neurosurgery, University of Michigan, Ann Arbor. Phone: (734) 647-0926

Chia-Ying Lin,

Spine Research Laboratory, Department of Neurosurgery, University of Michigan Medical School, Phone: (734) 615-0371; Fax: (734) 763-7322

Scott J. Hollister

Department of Mechanical Engineering, Scaffold Tissue Engineering Group, Department of Biomedical Engineering, Spine Research Laboratory, Department of Neurosurgery, Department of Surgery, University of Michigan, Ann Arbor. 2208 Lurie Biomedical Engineering Building, 1101 Beal Ave, Ann Arbor, MI 48109, Phone: +1-734-6479962, Fax: +1-734-6474834

Heesuk Kang: kanghs@umich.edu; Chia-Ying Lin: lincy@umich.edu; Scott J. Hollister: scottho@umich.edu

Abstract

Tissue engineering scaffolds play critical roles in skeletal tissue regeneration by supporting physiological loads as well as enhancing cell/tissue migration and formation. These roles can be fulfilled by the functional design of scaffold pore architectures such that the scaffold provides proper mechanical and mass transport environments for new tissue formation. These roles require simultaneous design of mechanical and mass transport properties. In this paper, a numerical homogenization based topology optimization scheme was applied to the design of three dimensional unit microstructures for tissue engineering scaffolds. As measures of mechanical and mass transport environments, target effective bulk modulus and isotropic diffusivity were achieved by optimal design of porous microstructure. Cross property bounds between bulk modulus and diffusivity were adapted to determine feasible design targets for a given porosity. Results demonstrate that designed microstructures could reach cross property bounds for porosity ranging from 30% to 60%.

Keywords

Tissue scaffold design; Microstructure; Homogenization; Topology optimization; Effective diffusivity

1 Introduction

The tissue engineering approach for repairing diseased or damaged tissues utilizes biomaterial scaffolds delivering biologics, including cells, genes, and/or proteins. Isolated

donor cells are cultured on a scaffold and the cell-scaffold construct is implanted into a tissue defect site (Langer and Vacanti 1993; Kim and Mooney 1998). During in vitro cell culture and after implantation, a scaffold serves several roles in tissue regeneration. It preserves three-dimensional space to guide tissue formation, maintains structural integrity under physiological loading conditions, and facilitates transport of nutrients and metabolic wastes (Hollister 2005). These scaffold roles are influenced by its internal architecture including porosity, pore size, and interconnectivity. In turn, the pore architecture affects functional characteristics such as mechanical modulus and diffusivity/permeability (Chu 2002). Thus, the goal of scaffold design should be to find a pore geometry, or microstructure that best achieves a desirable functional environment for a regenerated tissue.

The appropriate properties a scaffold should provide are generally tissue specific and, moreover, the properties often conflict with each other. It is hypothesized that scaffold elastic or aggregate modulus should match those of healthy tissues at the defect (Hutmacher 2001), which spans 10 ~ 1500 MPa (elastic modulus) for trabecular bone (Goulet et al. 1994) and 0.5~3.0 MPa (aggregate modulus) for articular cartilage (Boschetti et al. 2004; Demarteau et al 2006). While satisfying these mechanical requirements, bone tissue engineering scaffolds should be designed with high diffusivity, permeability or porosity for better cell migration and biologics transport. However, scaffolds for cartilage regeneration are often designed with limited transport property due to the avascular and low metabolic nature of cartilage (Malda et al. 2003).

One way to achieve these diverse design goals is adapting optimization schemes in hierarchical scaffold design (Hollister 2005). In the hierarchical scaffold design scheme, unit microstructures, or unit cells (structural unit, not biological cells) are chosen from unit cell libraries and assembled to form a scaffold global shape that fits into anatomical defects. The mechanical and mass transport properties of the scaffold are computed using the homogenization method based on double-scale asymptotic expansion (Sanchez-Palencia 1980). Pore architectures can be designed with predefined geometries such as three orthogonal cylindrical pores or spherical pores. Hollister et al. (2002) optimized pore diameters of scaffolds with three orthogonal cylindrical pores with homogenization method and empirically fitted polynomials that relate pore diameters and the effective stiffness tensor. Transport requirements were considered by imposing a lower bound constraint on porosity.

In more general cases, however, new microstructures with target properties can be sought using topology optimization (Bendsoe and Kikuchi 1988; Sigmund 1994a; Sigmund 1994b). Topology optimization distributes material within a unit microstructure such that the final structure meets specified design targets. Lin et al. adapted the topology optimization to find scaffold microstructures that achieved target anisotropic elastic constants (Lin et al. 2004). Lin and Hollister (Lin 2005; Hollister and Lin 2007) further extended the method by introducing the effective permeability to the optimization scheme to design scaffolds with maximized permeability. However, the permeability was not coupled with the mechanical property in the optimization procedure, so that maximizing permeability could affect the mechanically optimized microstructure.

Recently, several multifunctional material design schemes based on the topology optimization have been proposed. Guest and Prevost (2006) proposed a general 3D microstructure design scheme using the topology optimization method to achieve maximized bulk modulus and isotropic permeability. They optimized microstructures by differentially weighting mechanical and transport terms in the objective, allowing designers to tailor the material properties. de Kruijf et al (2007) found optimal structures with maximized bulk modulus and thermal conductivity by minimizing both mechanical and thermal compliance in 2D. The authors explored Pareto optimality by varying weights for mechanical and transport properties. Challis et al (2008), by utilizing level set method, presented the design of isotropic unit structures with maximized bulk modulus and isotropic conductivity. The authors also explored design changes with the different combinations of weighting factors.

The design of multifunctional material structures with maximized properties is gaining interest in many engineering fields. Tissue engineering scaffolds, however, must be tailored to a wide range of mechanical and mass transport properties, included cross property relationships that fall well within the interior of cross-property bounds, not just on the boundaries of the cross-property bounds. For example, cartilage needs low mass transport and mechanical properties (Kemppainen and Hollister, 2009) which lay well within the interior of the mass transport and mechanical cross-property bounds.

Thus, the goal of this study was to explore possible microstructure designs with various combinations of effective bulk moduli and diffusivities. In order to design microstructures with ranges of mechanical and mass transport properties, we adapted a local microstructure topology optimization scheme based on the SIMP method for target optimization. The target properties were chosen within known cross-property bounds connecting effective bulk modulus and isotropic diffusivity. Various microstructures were designed and utilized within actual tissue engineering scaffolds. A porous biodegradable interbody fusion cage was designed as a biomedical application of multifunctional microstructures by integrating the result from global topology optimization and the local microstructure optimization. The resulting integrated local and globally designed structures were the built using solid free-form fabrication techniques.

2 Materials and Methods

2.1 Homogenization of diffusivity and elasticity

The homogenization method determines effective macroscopic properties from an analysis of a representative microstructure of a porous media or composite material assuming periodicity (Sanchez-Palencia 1980). The analysis responses at a local level are averaged to give the effective properties at global scale. A major assumption is separation of the scales between macrostructure and microstructure. Based on this assumption, a small variable, ε, for the ratio between microscopic length scale and macroscopic length scale can be defined as,

$$\varepsilon = \frac{x_i^0}{x_i^1} << 1 \tag{1}$$

where x_i^0 is a spatial variable for macrostructure and x_i^1 is the microscopic spatial variable. Field variables are asymptotically expanded with respect to the microscopic scale and a hierarchical gradient can be defined with respect to the macroscopic length scale by the chain rule. Substitution of the expanded field variables and the hierarchical derivatives into the governing equilibrium equations leads to macroscopic and microscopic equilibrium equations. The microscopic equation can be solved by applying unit gradients of the macroscopic variables under the assumption of the periodicity of the microstructure and properties. The governing equations for local diffusivity are:

$$\frac{\partial}{\partial x_i^1} D_{ij} \frac{\partial \chi^p}{\partial x_j^1} = \frac{\partial}{\partial x_i^1} D_{ip} \tag{2}$$

where D_{ij} is the local diffusivity and χ^p is the characteristic concentration resulting from the p^{th} unit concentration gradient (p=1,2, and 3).

The governing equations for local elasticity are:

$$\frac{\partial}{\partial x_j^1} C_{ijkl} \frac{\partial \chi_k^{pq}}{\partial x_l^1} = \frac{\partial}{\partial x_j^1} C_{ijpq} \tag{3}$$

where C_{ijkl} is the localized elasticity and χ_k^{pq} is the characteristic displacement resulting from the unit strain in pq-direction (pq=11, 22, 33, 12, 23, and 31).

From the responses of the microscopic equation, the homogenized diffusion properties are calculated as:

$$D_{ij}^H = \left\langle D_{ik} \left(\delta_{jk} - \frac{\partial \chi^j}{\partial x_k^1} \right) \right\rangle \tag{4}$$

where D_{ij}^H is the homogenized diffusivity, D_{ik} is local diffusivity, δ_{jk} is the kronecker delta, and $\langle \cdot \rangle$ denotes volume average of a quantity.

The homogenized elasticity properties are calculated as:

$$C_{ijkl}^H = \left\langle C_{ijpq} \left(\delta_{kp}\delta_{lq} - \frac{\partial \chi_p^{kl}}{\partial x_q^1} \right) \right\rangle \tag{5}$$

where C_{ijkl}^H is the homogenized elasticity tensor, and C_{ijkl} is the localized elasticity.

The microscopic equations can be solved numerically with the finite element method. The characteristic responses to the applied global gradients and periodic boundary conditions compose a local structure matrix. Multiplication of the local property matrix and the local structure matrix averaged over the microstructural volume gives the homogenized property.

The unit cell domain was discretized into voxel elements, or 8-node hexahedral elements to evaluate the homogenized properties using the finite element method. Periodic boundary

conditions were implemented by assigning equivalent nodal constraints by assuming symmetries in the unit cell geometry and the local properties (Auriault 2001; Hassani and Hinton 1996). In this way, only one-eighth domain was considered as design domain. The element-by-element preconditioned conjugate method was used as a solver for the finite element analysis of the microscopic problems because of its efficiency when dealing with large degrees of freedom.

2.2 Theoretical Bounds and Cross-Property Bounds

There are upper and lower bounds on the effective properties for composite material for given material volume fractions. Hashin and Shtrikman derived well-known bounds for isotropic magnetic permeability and bulk/shear moduli using variational principles (Hashin and Shtrikman 1962; Hashin and Shtrikman 1963). The theoretical bounds for the effective magnetic permeability also hold for the effective diffusivity owing to the mathematical equivalency. For isotropic, three dimensional, solid-void phase composites, the upper bound on the effective bulk modulus and the effective diffusivity can be expressed in terms of the solid phase volume fraction and phase properties.

$$K_{\max}^{iso} = \frac{(3/4)\rho K G}{(1-\rho)K + (3/4)G} \tag{6}$$

$$D_{\max}^{iso} = \frac{2(1-\rho)D}{2+\rho} \tag{7}$$

where ρ is solid phase volume fraction, K and G are the bulk and shear moduli of solid phase and D is a free isotropic diffusion coefficient of a solute in the fluid phase. Fig. 1 illustrates the bounds on the relative isotropic diffusivity and bulk modulus in terms of solid phase volume fraction. The competition between elasticity and mass transport is obvious from the plots.

When multiple, conflicting properties are considered simultaneously, there are cross-property bounds that connect those properties through the microstructure. Such cross-property bounds provide an achievable range of one property if the other is known. For cross-property bounds that link bulk modulus and isotropic conductivity (diffusivity), Gibiansky and Torquato derived the sharpest known cross-property bounds using translation methods (Gibiansky and Torquato 1996). The cross-property upper bounds for an ill ordered solid-void(fluid) phase ($K_2 / K_1 = \infty$ and $D_2 / D_1 = 0$) can be defined in diffusivity-bulk modulus phase plane with a hyperbola segment that passes through three points, $(D_{\max}^{iso}, 0)$, $(0, K_{\max}^{iso})$ and $((1-\rho)D_1, \rho K_2)$, where D_1 and K_1 (= 0) are the diffusivity and bulk modulus of the void phase, D_2 (=0) and K_2 are the diffusivity and bulk modulus of the solid phase, and $D_{\max}^{iso}$ and $K_{\max}^{iso}$ are defined in equations (6) and (7). Fig. 2 illustrates an example for the cross-property bounds in the diffusivity-bulk modulus phase for an ill ordered composite where $K_2 / K_1 = \infty$, $D_2 / D_1 = 0$ and 50% porosity. As can be seen, lower bounds are straight lines parallel to the axes. All feasible elasticity/diffusivity designs for a 50% porous material must lie within the lines in Fig. 2. As noted by the authors, their cross-property bounds hold for both isotropic and cubic symmetric composites.

2.3 Topology optimization problem statement

Microstructure topology optimization computes the optimal topology of scaffold microstructure by distributing material density within the unit cell domain under design objectives and constraints (Sigmund 1994a; Sigmund 1994b). The design domain is discretized with the finite elements assigned with density values, ranging from 0 through 1. In this relaxed problem, material laws should be defined to relate element densities and local material properties. In addition, the intermediate density values are penalized to have a final discrete design. The most common local material law is the Solid Isotropic Microstructure with Penalization (SIMP) (Bendsoe 1989). We utilized the SIMP method for elasticity:

$$C_{ijkl} = \rho^p C^{base}_{ijkl}, (p > 1) \tag{8}$$

where C_{ijkl} is the element stiffness tensor, ρ is the element density, p is a penalization factor, and C^{base}_{ijkl} is the stiffness tensor for the base material. For the diffusivity, a SIMP-like material law can be applied to the interpretation of the intermediate densities with penalization,

$$D_{ij} = (1-\rho)^p D^{base}_{ij}, (p > 1) \tag{9}$$

where D_{ij} is the element diffusivity tensor, ρ is the element density, p is penalization factor, and D^{base}_{ij} is the free diffusivity tensor for the fluid phase. With the local material laws defined for both stiffness and diffusivity, the objective function and sensitivity derivatives are derived with respect to material density ρ, and the optimization problem can be solved by updating ρ at each iteration. For the phase base material, we used unit isotropic diffusivity, D=1 for the void phase. For the base material solid phase, we chose Poisson's ratio equal to 1/3 with a Young's modulus of 1, which yields a bulk modulus of 1. In this case, the designed properties could be easily compared within the cross-property bounds normalized to base material properties.

In order to tailor the material properties directly, the optimization problem was defined to minimize the error between the target and the effective bulk moduli and diffusivities, with constraints on porosity:

$$\begin{aligned} &\text{minimize} \quad f = w_1\left(\frac{K^H}{K^*} - 1\right)^2 + w_2\left(\frac{D^H}{D^*} - 1\right)^2 + w_3 f_{cubic} \\ &\text{subject to } \phi_{\text{lb}} \le \sum_{i=1}^{N} \frac{1-\rho_i}{N} \le \phi_{\text{ub}}, \\ &0 < \rho_i \le 1 \end{aligned} \tag{10}$$

where K^H is the homogenized bulk modulus, K^* is the target bulk modulus, D^H is the homogenized isotropic diffusivity, D^* is the target isotropic diffusivity, f_{cubic} is the cubic error function and w_i (i=1,…,3) are weighting factors, ϕ_{lb} and ϕ_{ub} are the upper and lower bounds of porosity, ρ_i is i-th element density, and N is the total number of elements.

The cubic error function is defined to minimize the differences among three normal components, three off-diagonal terms, and thee shear terms in the stiffness tensor components, respectively.

$$f_{cubic} = \left(\frac{C^H_{2222}}{C^H_{1111}} - 1\right)^2 + \left(\frac{C^H_{3333}}{C^H_{2222}} - 1\right)^2 + \left(\frac{C^H_{1111}}{C^H_{3333}} - 1\right)^2 + \left(\frac{C^H_{2233}}{C^H_{1122}} - 1\right)^2 + \left(\frac{C^H_{1133}}{C^H_{2233}} - 1\right)^2 + + \left(\frac{C^H_{1122}}{C^H_{1133}} - 1\right)^2 + \left(\frac{C^H_{1313}}{C^H_{2323}} - 1\right)^2 + \left(\frac{C^H_{1212}}{C^H_{1313}} - 1\right)^2 + \left(\frac{C^H_{2323}}{C^H_{1212}} - 1\right)^2 \quad (11)$$

Heesuk: Please note that I changed the indices above to reflect the correct index notation for the shear terms, Scott where C^H_{ijkl} are the components of the homogenized stiffness tensor.

This multiobjective formulation can be easily converted to a formulation in which one of the target properties is optimized while the other is constrained.

Topology optimization, in its relaxed formulation, still requires additional treatments to avoid known numerical instabilities such as checkerboard patterns and mesh dependencies (Sigmund and Petersson 1998). We applied a nonlinear filtering scheme to the sensitivity derivatives to prevent checkerboard patterns and mesh dependency as proposed by Sigmund (Sigmund 1994a). Based on element resolution, a filter radius of 3 elements was chosen to maintain a minimum physical feature size (what is this feature size?) for the 40×40×40 element unit cells. When the mesh resolution was increased to 60×60×60, the filter radius was increased to 4 elements to maintain the minimum physical feature size. Finally, to solve the optimization problem, the Method of Moving Asymptotes (MMA) was adopted to provide greater efficiency in solving problems with a large number of variables and a small number of constraints (Svanberg 1987).

3 Results

Our results demonstrated that the properties of the microstructures can be tailored to meet various scaffold requirements such as stiffness and mass transport using topology optimization with SIMP interpolation and sensitivity filtering. Target design points were chosen close to the cross-property upper bounds. Fig 3 illustrates various microstructural architectures obtained in this study and the achieved properties are presented in Table 1. The mesh resolution for microstructures (A), (C), (E), (G), and (F) was 60×60×60, and the mesh resolution for the other microstructures was 40×40×40. The designed microstructures were identified within the cross-property bounds in Fig 4.

The porosities of the designed microstructures satisfied the constraints despite the lack of an exact match in the corresponding cross-property bounds. This is because the porosity constraints were set at a small range around the target porosity. For example, the porosity constraints were set between 48% and 52% to design for the 50% cross-property bounds. .

Nonetheless, there was excellent agreement between the target and designed bulk moduli and diffusivities (Fig 5).

Because of the theoretical cross-property bounds for 50~60% porosities, the maximum normalized diffusivities are 0.4 and 0.5, respectively. Thus, we may consider diffusivity over 0.3 as high diffusivity for 50~60 % porosity materials.

3.1 Microstructures with High Diffusivity

Microstructures with relatively high diffusivity designed for either 50% or 60% porosity approached the cross-property upper bound, as depicted in Fig 3-D through Fig 3-H. The properties of the microstructures illustrated in these figures were isotropic. It should be noted that the designed microstructures have different topologies while the achieved properties were close to each other. Interestingly, the property pair of the microstructure in Fig 3-F is the closest to the cross-property upper bound, implying that the structure is optimal. Furthermore those microstructures designed to have 60% porosity showed lower bulk modulus of approximately 0.1 of that of the solid phase. When the structures were specified within cross-property bounds, both structures again have near optimal properties because the properties are close to the upper bounds (Fig 4).

3.2 Microstructures with Low Diffusivity

Microstructures designed to achieve low diffusivity for 30% porosity were also close to the corresponding cross-property upper bounds (Fig 3-A through C). The optimized structures have thick members across the diagonal of the unit cell domain to achieve high bulk modulus, and small pore diameters to decrease diffusivity. The normalized diffusivities of these microstructures were between 0.12 and 0.17 (Table 1). These low diffusivity structures are also close to the upper cross-property bounds due to high bulk modulus (Fig 4).

3.3 Microstructure targeting Low Diffusivity and Low Bulk Modulus

A microstructure designed with low diffusivity and low bulk modulus achieved the target properties although it contains significant intermediate densities. For cartilage tissue engineering applications, microstructures with low modulus and low diffusivity are desired. Such microstructures within the interior of the cross property bounds, well away from the upper limits that have been the target of most multiphysics microstructural topology optimization applications. These targets present significant challenges as the increase of material will increase bulk modulus (although decreasing diffusivity) and vice versa, the opposite of the design goal.

To eliminate the intermediate densities, we used post processing. A low diffusivity and low bulk modulus microstructure was designed by targeting a diffusivity of 0.1 and a bulk modulus of 0.1. However, the result of the post processing, (diffusivity of 0.26 and bulk modulus of 0.1), changed the very properties achieved. The application of a threshold to the intermediate densities interpolated by SIMP model made the properties shift towards the cross-property upper bounds.

One interpretation for the intermediate densities is that the algorithm converged to local minimum before all densities were penalized. Thus, the convention of Sigmund's continuation method was employed to avoid convergence to a local minimum (Sigmund 1994a). However as expected, this essentially heuristic approach could not sufficiently penalize the intermediate densities: the final mechanical and transport properties are a diffusivity of 0.12 and a bulk modulus of 0.1, which is not a totally satisfactory solution to the problem due to the intermediate densities. The full structure and $1/8^{th}$ of the structure are shown in Fig 6-A and Fig 6-B, respectively. In addition, representative cross-sectional view of the density distribution were illustrated in Fig 6-C. There are significant amounts of grey elements at convergence, which may indicate local minima. There are very weak connections between large spheres at the corners.

3.4 Microstructures with the same porosity but different bulk modulus and diffusivity

A particular strength of the target optimization is the capability to create microstructures of the same porosity, but with a range of bulk modulus and diffusivity. We successfully designed microstructures with 45~50% porosities (Fig. 7) that had diffusivities ranging from 16% to 33% and effective bulk moduli ranging from 12% to 24% of base diffusivity and bulk moduli, respectively. This reflects the algorithms ability to distribute the same amount of material in different layouts to attain dramatically different effective mechanical and mass transport properties. The microstructures in Fig 7 can be used to experimentally investigate the sole effect of material distribution on load bearing and mass transport without the confounding variation of changing porosity.

3.5 Application in Tissue Engineering: Microstructures for Spinal Fusion Devices

There are many potential clinical applications for topology optimized biomaterial scaffolds. One application is spinal fusion, which requires a scaffold that combines sufficient load bearing with high mass transport to enable bone formation. Spinal fusion has been successfully applied in the treatment of the degenerative disc diseases such as radiculopathy and myelophathy (McAfee 1999). Disc degeneration may compress nerve roots, resulting in the chronic neck and low back. By fusing vertebral bodies at the degenerative disc level, immediate recovery of disc height is ensured with pain relieve at the expense of reduced segment mobility. To overcome complications related to conventional metallic cages or non degradable polymeric cages, Lin et al. proposed a biodegradable porous interbody fusion cage design scheme using an integrated global and local topology optimization (Lin et al. 2004). This concept was applied to the design of biodegradable lumbar interbody fusion cages customized for a large animal study (Kang et al. 2008).

Scaffolds for tissue engineering must satisfy the need for a global scaffold shape or envelope with a distribution of designed microstructures. The global material density map is obtained by topology optimization of global anatomic structures to minimize compliance under physiological loads including flexion, extension, lateral bending and torsion. Then, microstructures with appropriate properties determined by local microstructure optimization are used replace segmented region based on the global density map. We successfully achieved a biodegradable interbody fusion cage for spinal fusion by replacing a material density distribution from the global structural topology optimization with our tailored

microstructures. To this end, a microstructure with high diffusivity (63%) but low bulk modulus (8%), and one with high bulk modulus (33%) but low diffusivity (17%) were designed.

The finite element model and the design domain for the optimal fusion cage were built based on medical images from a minipig (Fig 8-A). An example of density distribution resulting from the global topology optimization is illustrated in Fig 8-B. The design domain was segmented into three regions: solid (red region in Fig 8-C), high density (green region in Fig 8-C) and low density (clear region in Fig 8-C) regions. The detailed pore architecture of the fusion cage was implemented by replacing these regions with appropriate microstructures optimized with desired elasticity and diffusivity while satisfying a porosity constraint (Fig 8-C). Fig 8-D shows a final integrated design and its fabrication using a solid freeform fabrication technique that enables fabrication of complex geometries of porous fusion cage.

4 Discussion

It is hypothesized that scaffolds should provide mechanical and mass transport properties as close as possible to native tissues to enhance tissue regeneration (Hollister et al. 2009). As an active component, scaffolds should be able to provide a proper mechanical environment so as to maintain structural integrity at the defect site as well as transmit appropriate mechanical stimuli to newly generated tissues (Thomson et al. 1995, Hutmacher 2001, Simmons et al. 2001). In addition, scaffolds should provide appropriate mass transport conditions that can influence cell phenotype, tissue ingrowth, and nutrient conditions (Hollister et al., 2009;, Malda 2004). However, it is still unclear what optimal properties the scaffold should provide for the best tissue regeneration. For example, there have been inconsistent suggestions on the optimal pore size or porosities for tissue regeneration. Moreover, different levels of mass transport environment have been shown to result in differentiation to different cell types and degrees of tissue regeneration (Malda 2003).

In order to rigorously investigate correlations between functional environments and tissue regeneration, the ability to design scaffolds with controlled mechanical and mass transport properties is necessary. In this study, we were able to design microstructures for scaffolds with tailored mechanical and transport properties using topology optimization. Cross-property bounds provide on the feasible design space in the bulk modulus and diffusivity plane. Thus, topology optimization combined with cross-property bound can be a very useful design tool for creating microstructures with significant, controlled variations in mechanical and mass transport properties.

To avoid numerical instabilities inherent to the topology optimization, we applied the nonlinear sensitivity filter proposed by Sigmund (1994a). Filtering techniques are known to work well to avoid known instabilities such as checkerboard patterns and mesh dependence. The drawback of the filtering technique is that final structure often contains intermediate density values along solid-void boundaries due to the blurring effect of the filter. However, we found in many cases that 0–1 designs were achieved with the nonlinear sensitivity filter. We measured the convergence of the intermediate densities toward 0 or 1 by Eq (12).

$$R_{conv} = \frac{1}{N}\sum_{i=1}^{N}\frac{|\rho_i - 0.5|}{0.5} \quad (12)$$

R_{conv} approaches 1 as the intermediate densities are penalized toward either 0 or 1. With the SIMP topology optimization and sensitivity filter, we were able to obtain microstructures with an R_{conv} index over 0.95, which can be considered converged.

If R_{conv} is less than 0.95, the designed properties may shift towards upper cross-property bounds after post processing. From a practical view point, this may be beneficial because the premature solution still serves as a design choice. However, achieving a discrete solution is more desirable in terms of tailoring the material properties and creating a manufacturable design. In this regard, other techniques can be applied such as density filtering with a Heaviside step function (Guest et al, 2004) or addition of a nonlinear diffusion term to the objective function (Wang et al. 2004).

Many microstructure design studies have presented the composite or porous structures that are near or on the cross-property upper bounds (Guest and Prevost 2006; de Kruijf et al. 2007; Challis et al. 2008). In these previous works, two competing properties were maximized simultaneously. However, one of our main interests in this study was to design microstructures whose properties are far from the upper bounds.

Of particular interest in our study was the design of microstructures with low diffusivity and low bulk modulus. As presented in the result section, our design converges to a minimum. More often than not the R_{conv} index was less than 0.8. If we targeted a design point far from the upper cross-property bounds, R_{conv} index was even smaller. To evaluate the difficulty of achieving this inner design point, we tested three design points: (1) K=0.2 and D=0.3, (2) K=0.15 and D=0.2, and (3) K=0.1 and D=0.15. We used the same problem statement and control parameters for filtering until convergence at a (local) minimum was achieved.

The outer point or the point on the upper bounds was easily achieved with an R_{conv} index of almost 0.99. For the middle design point, the R_{conv} index was 0.93, which means the final design contained a blurry solid-void boundary. However, for the innermost design point case, the R_{conv} index was 0.71 and the structure exhibited a clear grey layer in addition to the black solid structure. This can be clearly noticed in the histogram plots (Fig 9) in which the number of elements having a given density are plotted in bins. The inner design point case had a large amount of elements containing density values of around 0.3~0.4. One explanation is that the presence of grey regions represents sub-microstructures that give more degrees of freedom in reaching the interior targets than can be reached using pure 0–1 designs. This is actually seen in the hierarchical structure of biologic tissues, which have feature sizes ranging from the nanometer to centimeter scale.

Another important factor is the consideration of the manufacturability. Particularly for the low diffusivity designs, the small holes develop to limit diffusivity. Considering the size of unit cells (typically around 1 mm) in the skeletal tissue scaffolds, the small holes may not be manufactured due to the limited fabrication resolutions. As for the optimization problem, it

would be interesting to control the member size as well as hole size as manufacturing control factors.

We also presented porous interbody fusion cage design using global-local integerated topology optimization technique (Lin et al. 2004), as an example of the clinical application of the microstructural topology optimization. A more critical role of the fusion cages is to restore original disc height to achieve nerve root decompression. Thus, the global density layout was found in the global topology optimization to maximize the overall stiffness of the device. Then, local microstructures were tailored to replace the global density map without changing the global porosity, which will facilitate transport properties of the fusion device. If one of the global design constraints limits excessive stress or strain on the interfacing bone, a low elastic modulus microstructure should be designed to match the global density map. The use of topology optimization to balance mechanical and mass transport properties is especially critical for fusion cages made from degradable polymers.

In our study, diffusivity was considered in this scaffold design because diffusion characteristics of the scaffold can govern overall cell migration and tissue regeneration as well as oxygen and nutrient delivery and metabolic waste removal. Thus, mathematical models of cell migration and tissue regeneration have adapted diffusion like equations (Anderson 1998; Adachi 2006). In addition, diffusivity and permeability of scaffolds are well correlated (Hollister et al. 2008). Moreover, there are known cross-property bounds on the effective diffusivity and bulk modulus, which can suggest feasible design characteristics.

As a temporary substitute for extracellular matrix, the scaffolds should provide tissue specific functional environments during new tissue formation. However, there is still little experimental data available regarding optimal effective scaffold properties for tissue regeneration. Moreover, conflicting findings have been reported regarding the effect of oxygen diffusion on cartilage regeneration, demonstrating the need for testing scaffolds with a range of designed properties (Malda 2004). In this regard, the microstructural topology optimization method, which is able to produce scaffolds with a range of designed properties, will provide more opportunities to investigate relevant scaffold properties.

Acknowledgement

This study was supported by funding from the NIH AR 053379 and DE 016129. The authors acknowledge the valuable advice and discussion by Dr. Jeong Hun Seo.

References

Adachi T, Osako Y, Tanaka M, Hojo M, Hollister S (2006) Framework for optimal design of porous scaffold microstructure by computational simulation of bone regeneration. Biomaterials 27(21): 3964–3972 [PubMed: 16584771]

Anderson ARA, Chaplain MAJ (1998) A mathematical model for capillary network formation in the absence of endothelial cell proliferation. Appl Math Lett 11(3): 109–114

Auriault JL, Lewandowska J (2001) Upscaling: Cell symmetries and scale separation. Transport Porous Med 43(3): 473–485

Bendsoe MP and Kikuchi N (1988) Generating Optimal Topologies in Structural Design Using a Homogenization Method. Comput Method Appl M 71(2):197–224

Bendsøe MP (1989) Optimal shape design as a material distribution problem. Struct Optimization 1(4): 193–202

Boschetti F, Pennati G, Gervaso F, Peretti GM, Dubini G (2004) Biomechanical properties of human articular cartilage under compressive loads, Biorheology 41:159–166 [PubMed: 15299249]

Challis VJ, Roberts AP, Wilkins AH (2008) Design of three dimensional isotropic microstructures for maximized stiffness and conductivity. Int J Solids Struct 45:4130–4146

Chu TMG, Orton DG, Hollister SJ, Feinberg SE (2002) Mechanical and in vivo performance of hydroxyapatite implants with controlled architectures. Biomaterials 23(5):1283–1293 [PubMed: 11808536]

de Kruijf N, Zhou S, Li Q, Mai YW (2007) Topological design of structures and composite materials with multiobjectives. Int J Solids Struct 44:7092–7109

Demarteau O, Pillet L, Inaebnit A, Borens O, Quinn TM (2006) Biomechanical characterization and in vitro mechanical injury of elderly human femoral head cartilage: comparison to adult bovine humeral head cartilage. Osteoarthr Cartilage 14:589–596

Gibiansky LV and Torquato S (1996) Connection between the conductivity and bulk modulus of isotropic composite materials. P Roy Soc Lond A Mat 452(1945):253–283

Goulet RW, Goldstein SA, Ciarelli MJ, Kuhn JL, Brown MB, Feldkamp LA (1994) The Relationship between the Structural and Orthogonal Compressive Properties of Trabecular Bone. J Biomech 27(4): 375–389 [PubMed: 8188719]

Guest JK, Prevost JH, Belytschko T (2004) Achieving minimum length scale in topology optimization using nodal design variables and projection functions. Int J Numer Meth Engng 61:238–254

Guest JK, Prevost JH (2006) Optimizing multifunctional materials: Design of microstructures for maximized stiffness and fluid permeability. Int J Solids Struct 43(22–23):7028–7047

Hashin Z, Shtrikman S (1962) A Variational Approach to Theory of Effective Magnetic Permeability of Multiphase Materials. J Appl Phys 33(10): 3125-

Hashin Z, Shtrikman S (1963) A Variational Approach to the Theory of the Elastic Behaviour of Multiphase Materials. J Mech Phys Solids 11(2): 127–140

Hassani B (1996) A direct method to derive the boundary conditions of the homogenization equation for symmetric cells. Commun Numer Meth En 12(3): 185–196

Hollister SJ (2005) Porous scaffold design for tissue engineering. Nat Mater 4(7):518–524 [PubMed: 16003400]

Hollister SJ, Maddox RD, Taboas JM (2002) Optimal design and fabrication of scaffolds to mimic tissue properties and satisfy biological constraints. Biomaterials 23(20): 4095–4103. [PubMed: 12182311]

Hollister SJ and Lin CY. (2007) Computational Design of Tissue Engineering Scaffolds, Computer Methods in App. Mech. and Eng 196:2991–2998.

Hollister SJ Lin CY Kang HS and Adachi T (2008) Computational Design and Simulation of Tissue Engineering Scaffolds, in Virtual Prototyping & Bio Manufacturing in Medical Application ed Bidanda B and Bartolo P Springer.

Hollister SJ, Liao EE, Moffitt EN, Jeong CG, Williams JM (2009) “Defining Design Targets for Tissue Engineering Scaffolds” in Fundamentals of Tissue Engineering and Regenerative Medicine, ed. Meyer U, Springer-Verlag.

Hutmacher DW (2001) Scaffold design and fabrication technologies for engineering tissues - state of the art and future perspectives. J Biomat Sci-Polym E 12(1): 107–124.

Kang H. Hollister SJ. LaMarca F. Lin CY. Situ Biodegradable Interbody Fusion Cage Design by the Integrated Global and Local Topology optimization – An example on designing Yucatan Minipig Lumbar Interbody fusion cage for large animal study. 54th ORS Annual Meeting; 2008.

Kemppainen JM, Hollister SJ (2009) Differential effects of designed scaffold permeability on chondrogenesis by chondrocytes and bone marrow stromal cells. Biomaterials In Press

Kim B, Mooney DJ (1998) Development of Biocompatible Synthetic Extracellular Matrices for Tissue Eng, TIBTECH 16:224–230

Langer R, Vacanti JP (1993) Tissue Engineering. Science 260(5110):920–926 [PubMed: 8493529]

Lin CY, Hsiao CC, Chen PQ, Hollister SJ (2004) Interbody fusion cage design using integrated global layout and local microstructure topology optimization. Spine 29(16):1747–1754 [PubMed: 15303018]

Lin CY, Kikuchi N, Hollister SJ (2004) A novel method for biomaterial scaffold internal architecture design to match bone elastic properties with desired porosity. J Biomech 37(5):623–636 [PubMed: 15046991]

Lin CY (2005) Solid-fluid mixture microstructure design of composite materials with application to tissue engineering scaffold design. Ph.D Thesis.

Malda J, Martens D, Tramper J, van Blitterswijk C, Riesle J (2003) Cartilage tissue engineering: Controversy in the effect of oxygen. Crit Rev Biotechnol 23(3):175–194 [PubMed: 14743989]

Malda J, Woodfield TBF, van der Vloodt F, Kooy FK, Martens DE, Tramper J, van Blitterswijk CA, Riesle J (2004) The effect of PEGT/PBT scaffold architecture on oxygen gradients in tissue engineered cartilaginous constructs. Biomaterials 25:5773–5780 [PubMed: 15147823]

McAfee PC (1999) Current concepts review: interbody fusion cages in reconstructive operations on the spine. J Bone Joint Surg Am 81:859–880 [PubMed: 10391552]

Sanchez-Palencia E (1980) Non-homogeneous Media and Vibration Theory. Berlin, Springer-Verlag.

Sigmund O (1994a) Design of Material Structures Using Topology Optimization, Ph.D Thesis.

Sigmund O (1994b) Materials with Prescribed Constitutive Parameters - an Inverse Homogenization Problem. Int J Solids Struct 31(17): 2313–2329.

Sigmund O, Petersson J (1998) Numerical instabilities in topology optimization: A survey on procedures dealing with checkerboards, mesh-dependencies and local minima. Struct Optimization 16(1): 68–75.

Simmons C, Meguid S, Pilliar R (2001) Differences in osseointegration rate due to implant surface geometry can be explained by local tissue strains. J Orthop Res 19(2):187–194 [PubMed: 11347689]

Svanberg K (1987) The Method of Moving Asymptotes - a New Method for Structural Optimization. Int J Numer Meth Eng 24(2): 359–373

Thomson R, Yaszemski M, Powers J, Mikos A (1995) Fabrication of biodegradable polymer scaffolds to engineer trabecular bone. J Biomat Sci-Polym E 7(1):23–38

Wang M, Zhou S, Ding H (2004) Nonlinear diffusion in topology optimization. Struct Multidiscip O 28:262–276

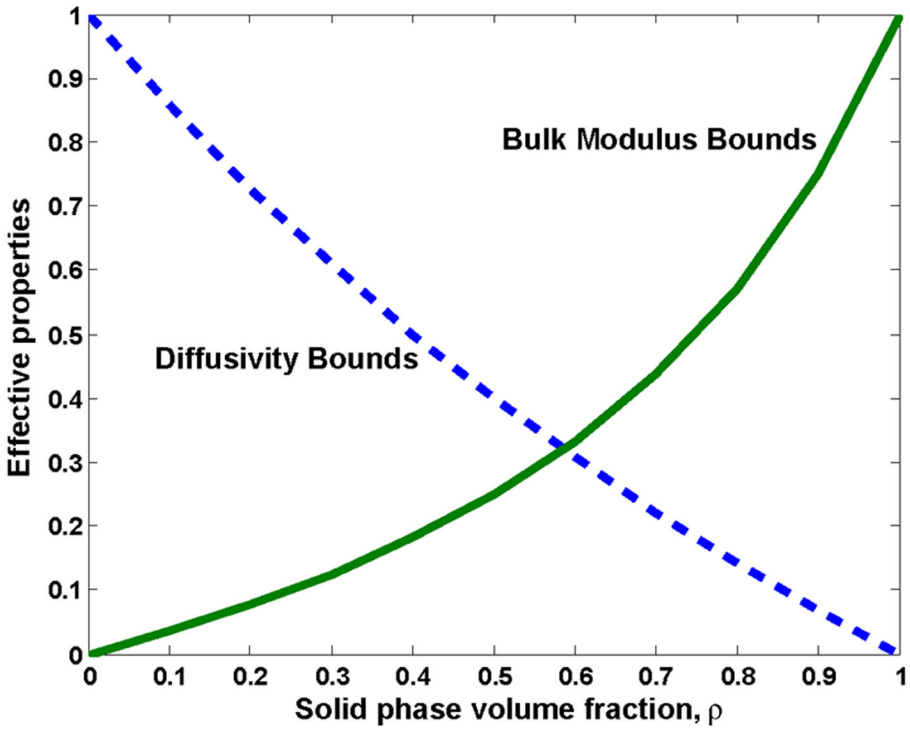

Fig 1.

Normalized theoretical bounds on isotropic diffusivity and bulk modulus plotted as a function of solid phase volume fraction

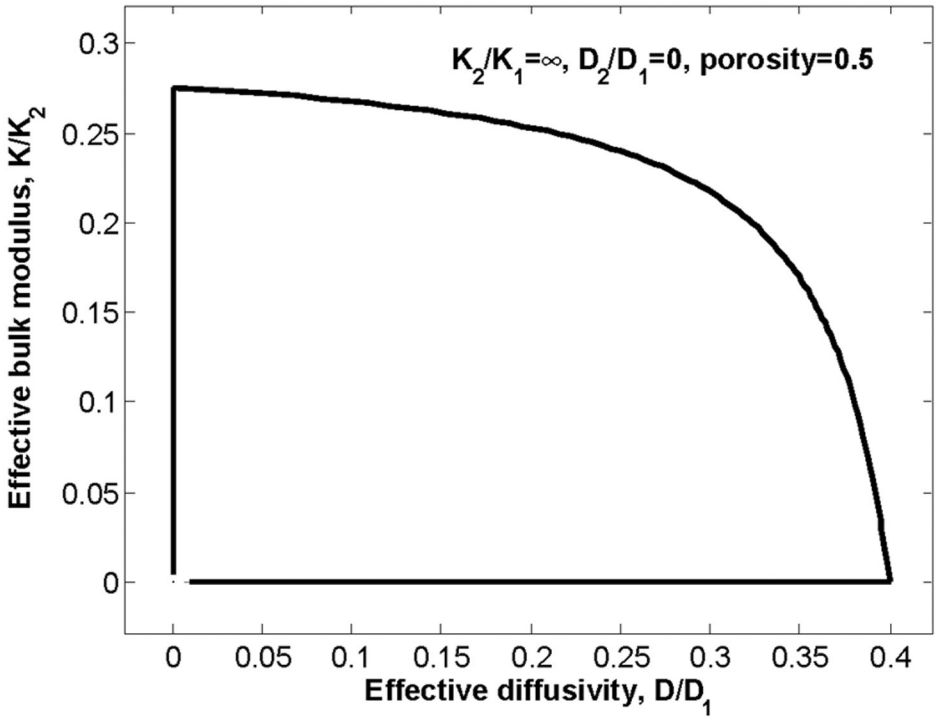

Fig 2.

An example of cross-property bounds on the effective bulk modulus and diffusivity for ill-ordered composite, adapted from Gibiansky and Torquato (1996)

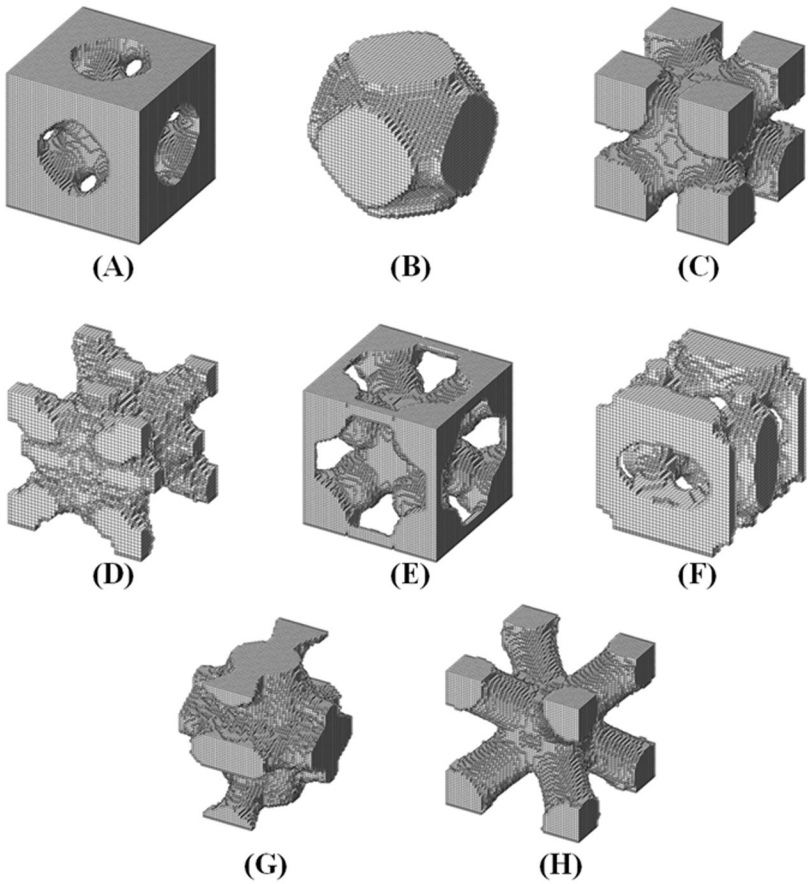

Fig 3.

Microstructures obtained by targeting bulk modulus and diffusivity close to the upper cross-property bounds, for 30% porosity (A,B and C), 50% porosity (D,E and F) and 60% porosity (G and H)

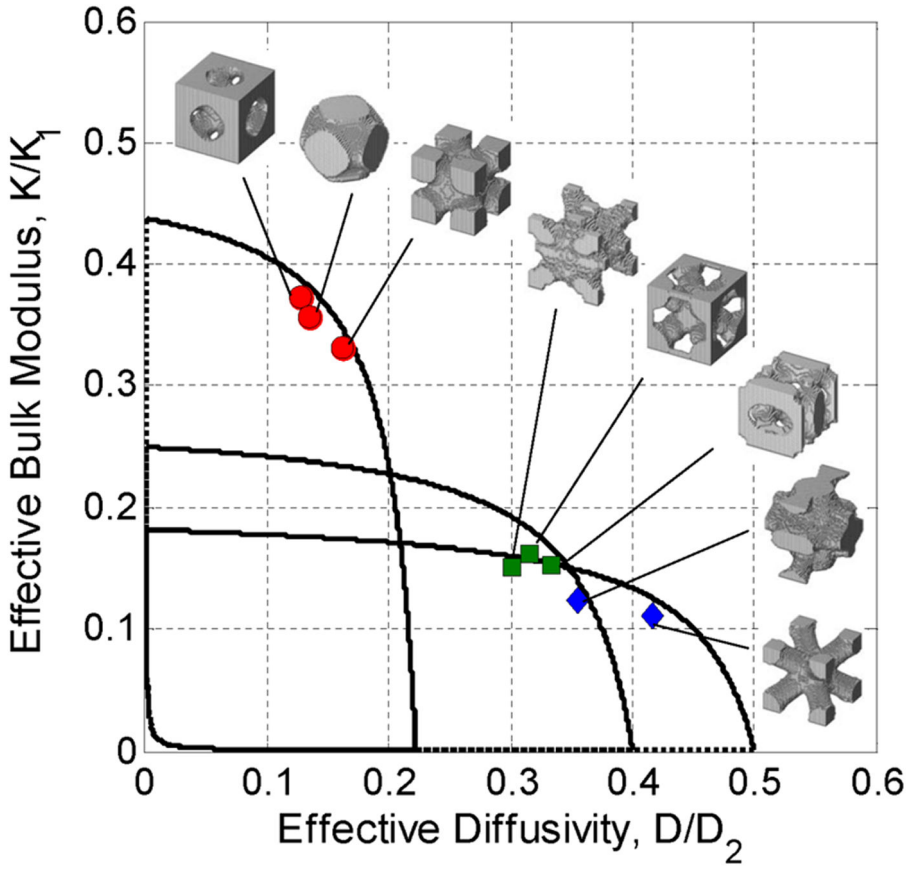

Fig 4.

Microstructures designed to achieve properties close to the upper cross-property bounds are specified within the cross-property bounds

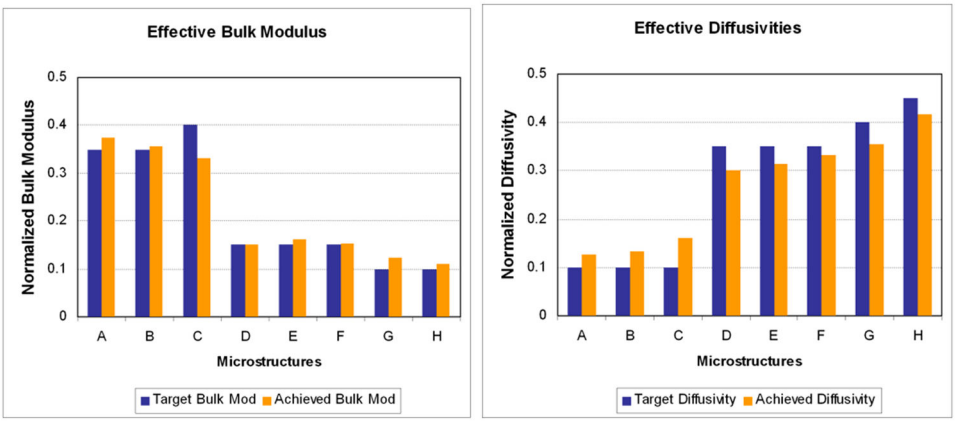

Fig 5.

The achieved bulk moduli (left) and diffusivities (right) were compared with target properties for the microstructures presented in Fig 3.

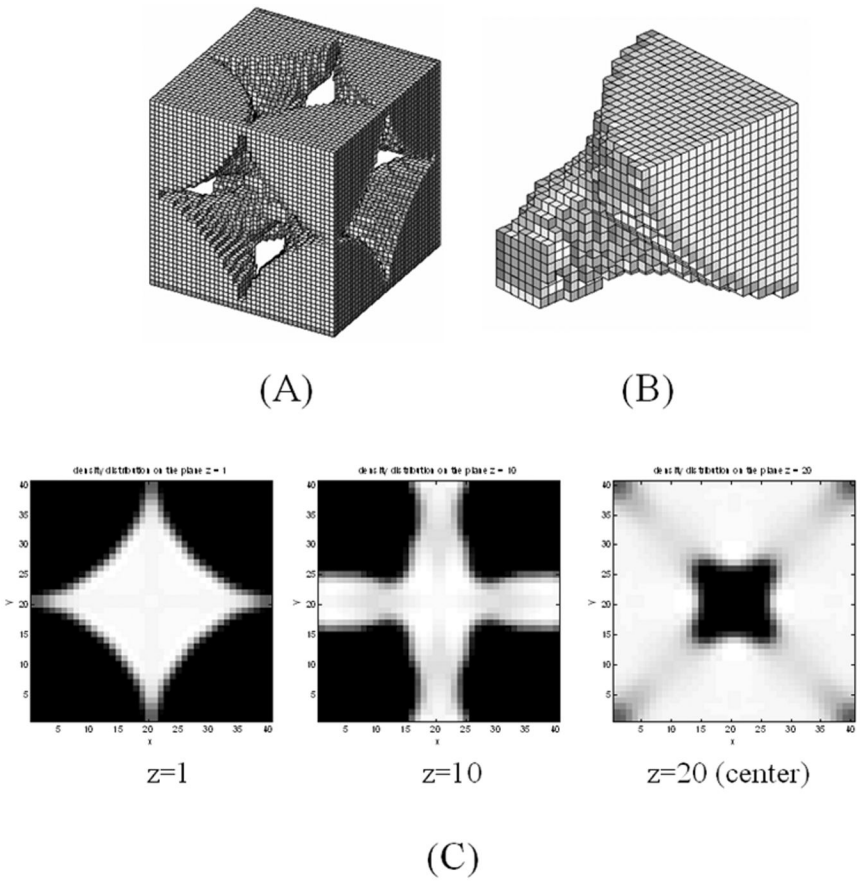

Fig 6.

(A) Microstructures with low diffusivity and low bulk modulus, (B) 1/8 of the designed microstructure and (C) representative cross-sectional view of the structure

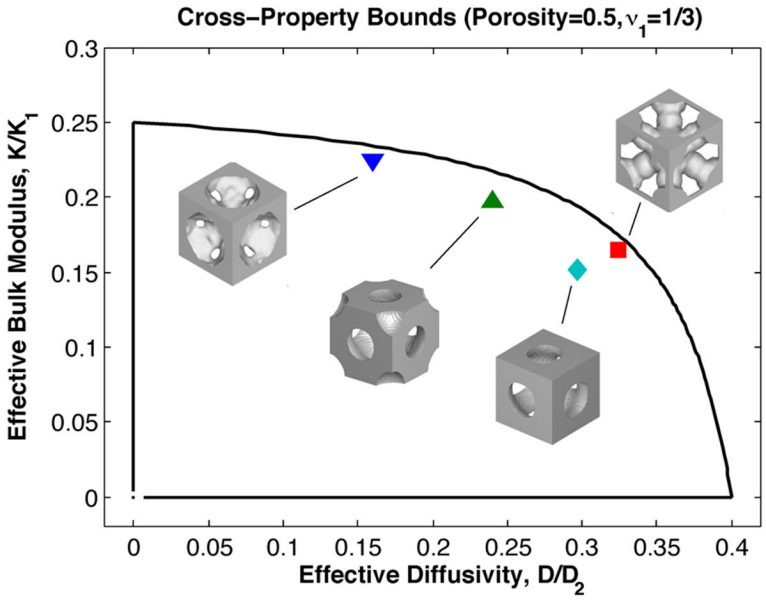

Fig 7.

Microstructure designs with ranges of diffusivities for 50% porosity

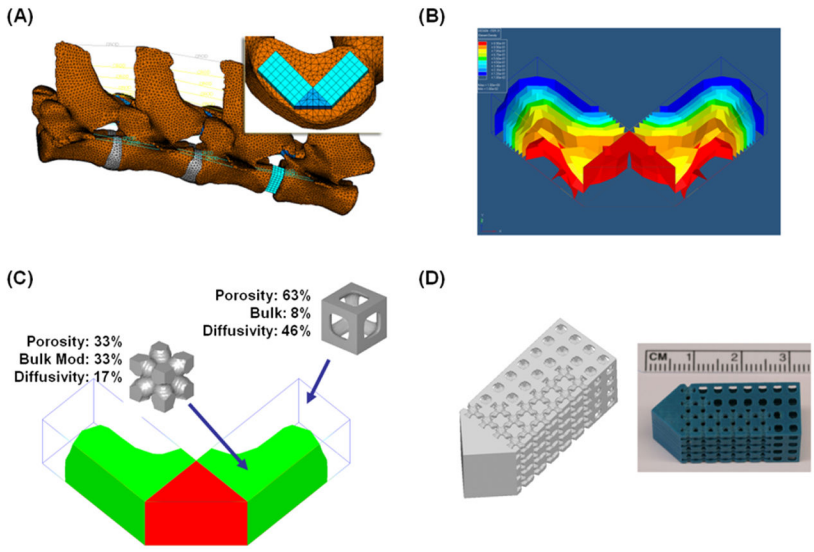

Fig 8.

(A) FE model for the global topology optimization including entire lumbar spine and specific design domain for the interbody fusion cage. (B) A density distribution within the design domain resulting from the global topology optimization. (C) The design domain was segmented into solid (red regions, zero porosity), high density (green regions, 33% porosity), and low density (clear regions, 63% porosity) regions. High density region was replaced with high modulus microstructure and low density region was replaced with low modulus microstructure. (D) Finial design of an optimal interbody fusion cage and its fabrication using solid freeform fabrication.

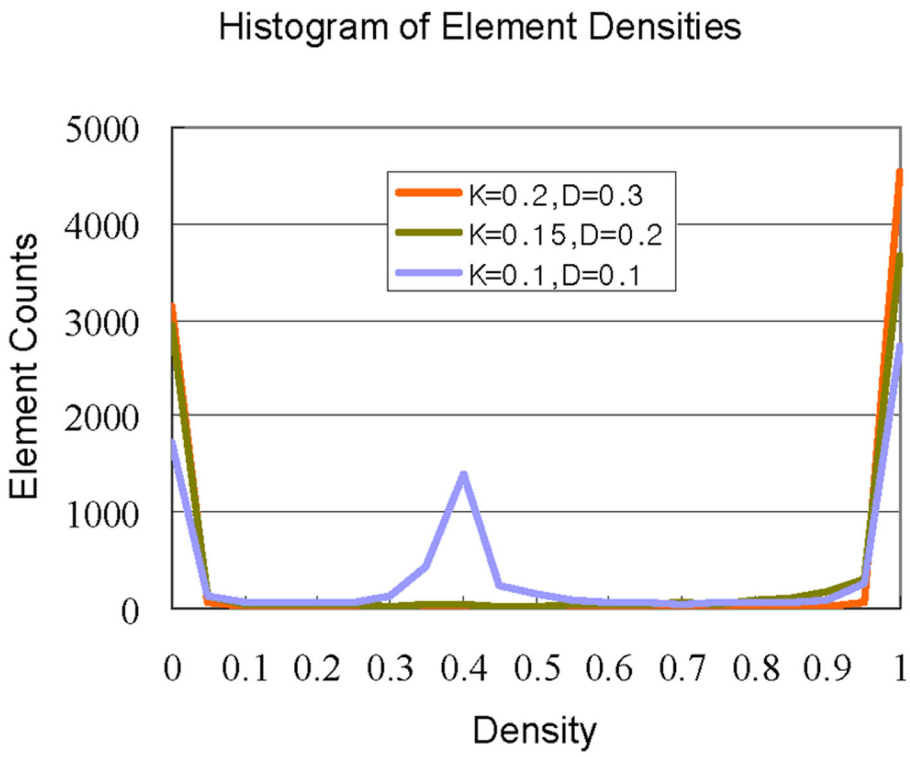

Fig 9.

Histograms of densities of three microstructure designs targeting K=0.2 and D=0.3, K=0.15 and D=0.2, and K=0.1 and D=0.1

Table 1

Properties of the designed microstructures in Fig 3

Microstructures	Porosity	Diffusivity	Bulk Modulus	Poisson's ratio
A	0.2825	0.1276	0.3734	0.2824
B	0.3030	0.1340	0.3565	0.2535
C	0.2935	0.1616	0.3317	0.2851
D	0.4831	0.3016	0.1512	0.2511
E	0.4828	0.3156	0.1624	0.2994
F	0.5037	0.3330	0.1522	0.2535
G	0.5802	0.3556	0.1246	0.1734
H	0.5882	0.4164	0.1114	0.3544